Supplementary materials

Improving carrier transport aided by Sb doping enables high effieicnt DMF-processed CIGSSe Solar cells with sub-thickness

Xuejun Xu [a], Yue Liu [a], Rutao Meng [a], Han Xu [a], Shuxia Wei [a], Zongjie Su [a], Jianpeng Li [a], Nan Wang [a], Shuai Shao [a], Yi Zhang [a, *]

[a] Institute of Photoelectronic Thin Film Devices and Technology, State Key Laboratory of Photovoltaic Materials and Cells, and Engineering Research Center of Thin Film Optoelectronics Technology, Ministry of Education, Nankai University, Tianjin 300350, China.

*Corresponding author.

E-mail addresses: yizhang@nankai.edu.cn (Yi Zhang)

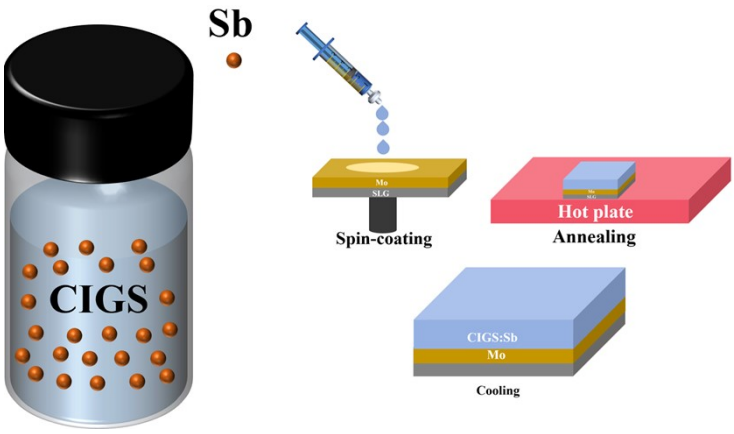

Fig. S1 The schematic diagram of the Sb doping CIGS precursor film preparation process.

Table S1. Elemental analysis of the composition of the precursor films with different Sb content from EDS results.

Original feeding Sb content (Sb/Cu%) in the Precursor film	**Measured Sb/Cu**	**Measured Ga/(Ga+In)**	**Measured Cu/(In+Ga)**
0%	0	0.30	0.92
2%	0.017	0.30	0.91
5%	0.044	0.31	0.91
8%	0.078	0.31	0.92

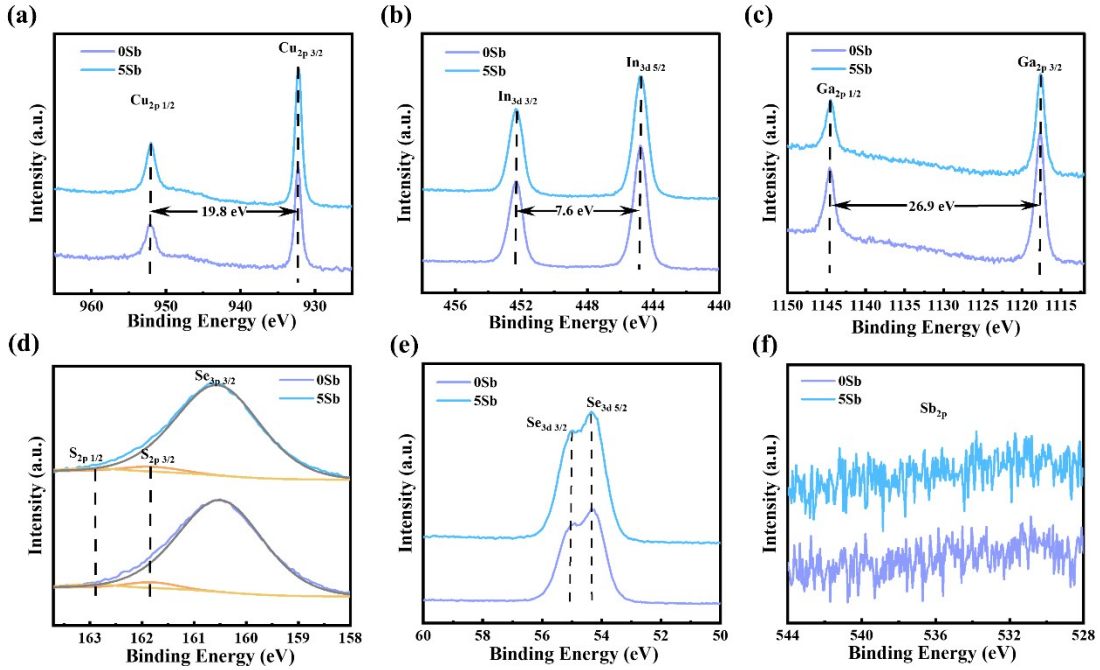

Fig. S2 (a) XPS spectra of Cu 2p core levels, (b) In 3d core levels, (c) Ga 2p core levels, (d) S 2p core levels and Se 3p core levels, (e) Se 3d core levels for the typical samples CIGSSe -0Sb and 5Sb.

Table S2. The XPS analysis of the typical samples CIGSSe-0Sb and 5Sb.

Absorber	Sb/Cu	Cu/(In+Ga)	Ga/(Ga+In)	Se/(S+Se)
CIGSSe-0Sb	0	0.95	0.33	0.92
CIGSSe-5Sb	0	0.98	0.26	0.97

Table S3. The EDS analysis of Sb/Cu for 5Sb precursor film at different selenization stages.

Sample	Selenization time	Sb/Cu	Sb (Sb percentages relative residual values normalized to 0 min)
5Sb Precursor film	0min	0.044	100%
	8min	0.035	79.5%
	15min	0.018	40.9%
	26min	0	Not detected

Supplementary Note 1.

For the evolution of Sb changes during the selenization process as shown in **Table S3**, the content of Sb gradually decreases, especially during the high temperature selenization (570 ℃) stage , and nearly no Sb can be detected in the final absorber film, which also indicate that Sb element nearly evaporated during the whole selenization as film crystallization proceeded.

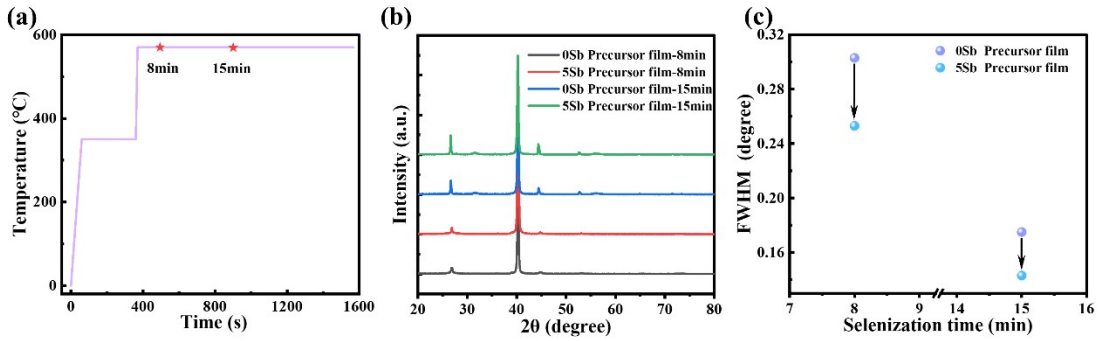

Fig. S3 (a) The temperature evolution during the CIGSSe selenization process. (b) The XRD patterns of CIGSSe precursor film doping 0 and 5% Sb (named as 0Sb and 5Sb precursor film) selenized at 8min and 15 min during the selenization. (c) The Gaussian fitting FWHM of (112) diffraction peak 0Sb and 5Sb precursor film at 8min and 15 min during the selenization.

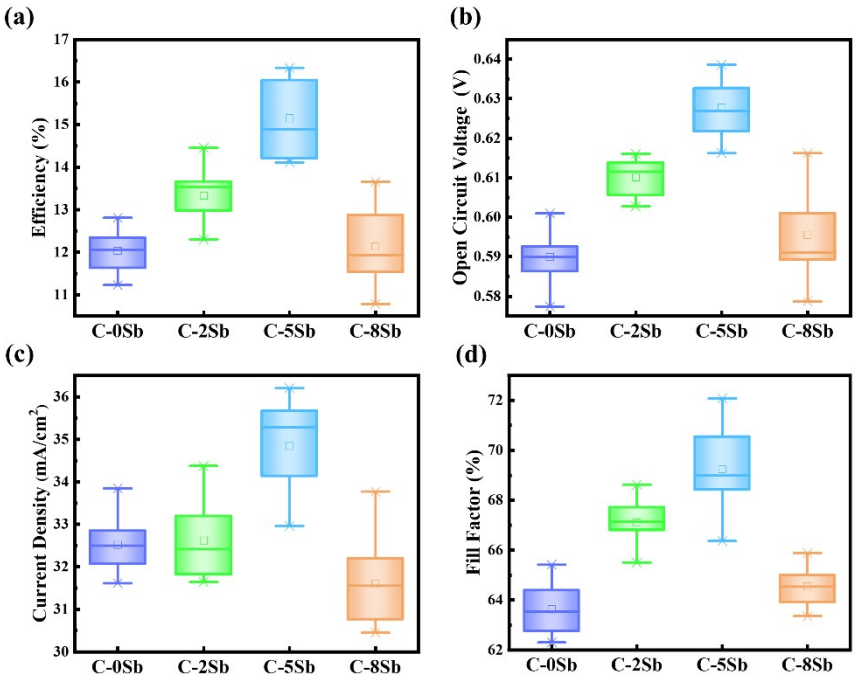

Fig. S4 Statistical results of (a) PCE, (b) V_{OC}, (c) J_{SC}, and (d) FF of cells C-0Sb, C-2Sb, C-5Sb and C-8Sb, respectively.

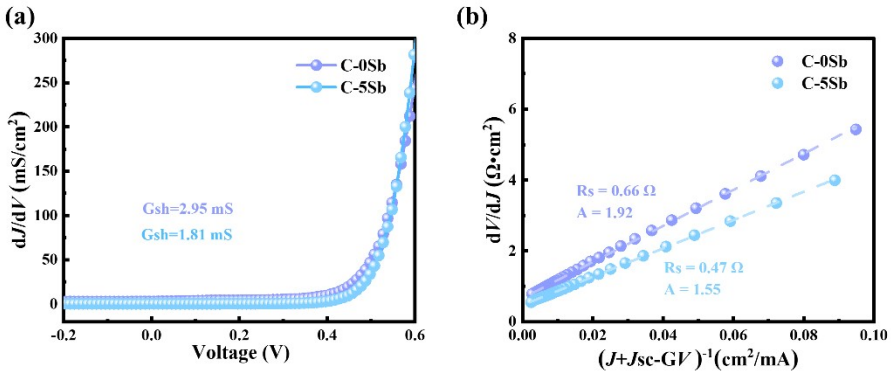

Fig. S5 (a) The Fitting results of the shunt conductance G. (b) Diode ideality factor (A) and series resistance (R_S) for cells C-0Sb and C-5Sb.

Supplementary Note 2.

The *J-V* characteristics of solar cells satisfy the single-exponential diode equation as follows [S1,S2]:

$$J = J_0 e^{[q/AKT(V - R_s J)]} + G_{sh}V - J_L \qquad (2\text{-}1)$$

in which the devices parameters, such as the shunt conductance (G_{sh}), series resistance(R_s), reverse saturation current density (J_0), and diode ideality factor (A), we can easily obtain the shunt conductance G from the figure dJ/dV versus Voltage. By fitting dJ/dV to the linear portion of the $(J+J_{SC}\text{-}GV)^{-1}$ curve, we can obtain the Diode ideality factor (A) and series resistance (R_S) for each sample.

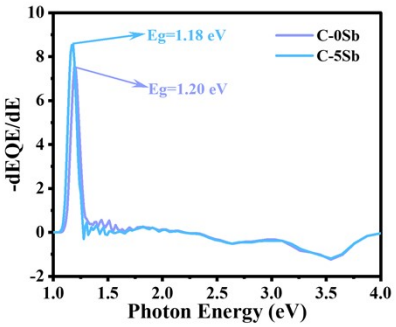

Fig. S6 The bandgap of cells C-0Sb and C-5Sb extracted from their EQE curves.

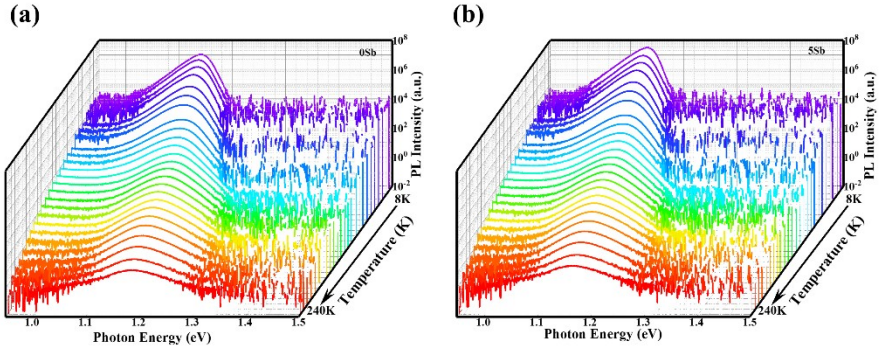

Fig. S7 The temperature dependent PL for samples (a) CIGSSe-0Sb and (b) 5Sb with temperature ranging from 8K to 240K excited by a 532nm continuous laser, and the excited power is 3W/cm^2.

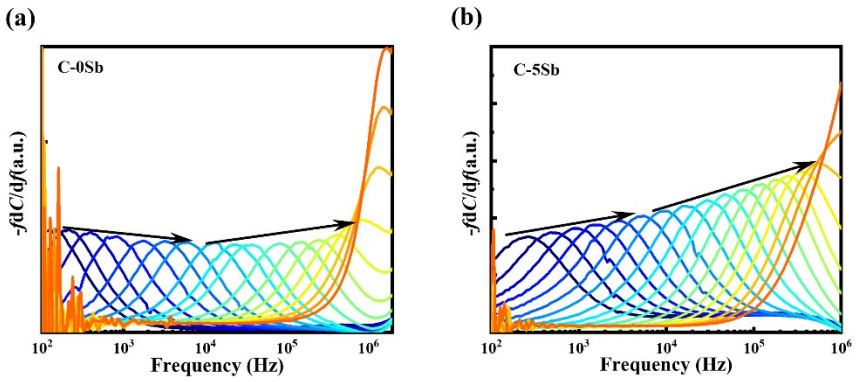

Fig. S8 $-f$dC/df spectra measured between 80 and 300 K with an interval of 10 K for cells (a) C-0Sb and (b) C-5Sb.

Supplementary Note 3.

For the admittance spectroscopy (AS) test analysis, the main principle can be explained by the following equation [S5,S6]:

$$\omega_0 = 2\pi\xi_0 T^2 exp(-E_a/kT) \tag{3-1}$$

where ω_0 is the circular frequency of the test signal at which the capacitive plunge occurs, ξ_0 is the pre-exponential factor comprising all temperature-independent terms. The above equation can be also rewritten as

$$\ln\left(\frac{w_0}{T^2}\right) = \ln(2\xi_0) - E_a/kT \tag{3-2}$$

A linear fit is performed with $\ln\left(\frac{w_0}{T^2}\right)$ as the dependent variable and 1/T as the independent variable. The slope is (E_a/k) and the intercept is $\ln(2\xi_0)$. The slope allows the energy level position of a defect to be calculated, while the intercept is calculated at the junction. The intercept is used when fitting the concentration of defect states at a given energy level with parameters, calculated as follows:

$$N_t(E(\omega)) = -\frac{V_{bi}}{qW_d}\cdot\frac{dC}{d\omega}\cdot\frac{\omega}{kT} \tag{3-3}$$

In which the Vbi and Wd can be obtained from the C-V curves for each sample.

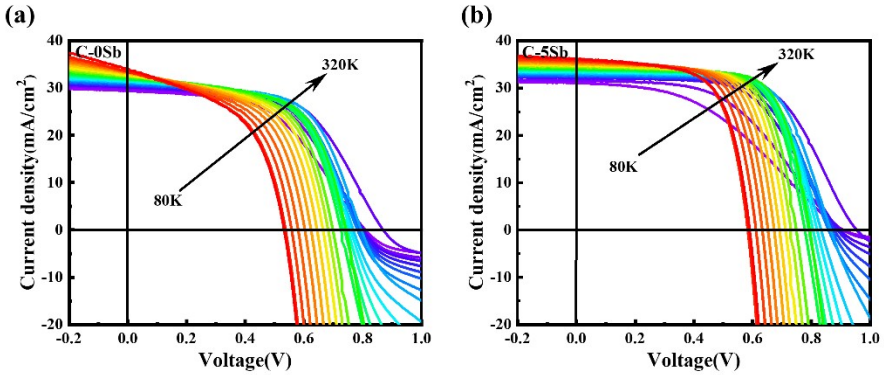

Fig. S9 Temperature dependent *J-V* curves of cells (a) C-0Sb, (b) C-5Sb.

Supplementary Note 4.

The analysis of the light *J-V* results leads to V_{OC} versus T to fit the activation energy E_A of the complex mechanism dominated by the space charge region, can be calculated by the following equation [S3,S4]:

$$V_{OC} = \frac{E_A}{q} - AkT/qln(J_{00}/J_L) \tag{4-1}$$

in which where A , J_{00} , and J_L are the diode ideality factor, reverse saturation current prefatory, and photocurrent, respectively. The intercepts of the linear extrapolation to 0 K provide activation energy E_A for each sample.

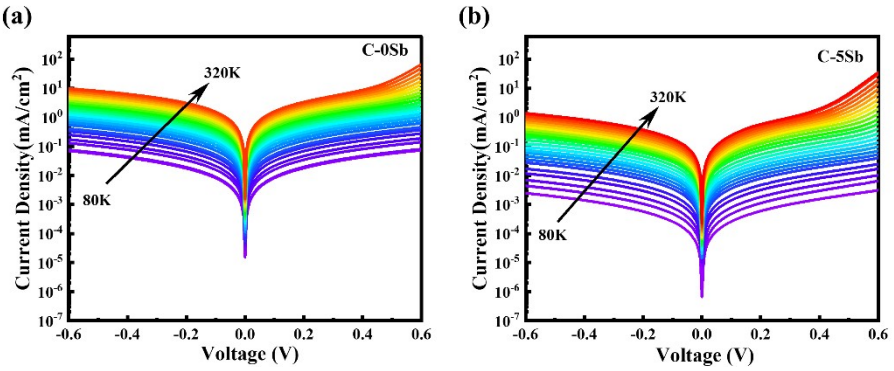

Fig. S10 The temperature-dependent dark-state *J-V* curves for cells (a) C-0Sb, (b) C-5Sb from 80K to 320K.

Table S4. The fitting results extracted from the TRPL curves of cells C-0Sb and C-5Sb.

Sample	A_1	τ_1/ns	A_2	τ_2/ns	τ_{ave}/ns
C-0Sb	0.89	0.79	0.11	3.91	1.97
C-5Sb	0.77	1.37	0.23	5.88	3.9

Supplementary Note 5.

The minority carrier lifetime can be fitted by the following biexponential equation [S7]:

$$I(t) = A_1 exp[-(t-t_0)]/\tau_1 + A_2 exp[-(t-t_0)]/\tau_2 \quad (5\text{-}1)$$

where A_1, A_2 are the amplitude coefficients representing magnitudes of the two decay processes, t_0 is the initial time, τ_1 and τ_2 are the time constants for the slow decay and fast decay, respectively. The average lifetime is defined as $\tau_{Avg} = (A_1\tau_1^2 + A_2\tau_2^2)/(A_1\tau_1 + A_2\tau_2)$.

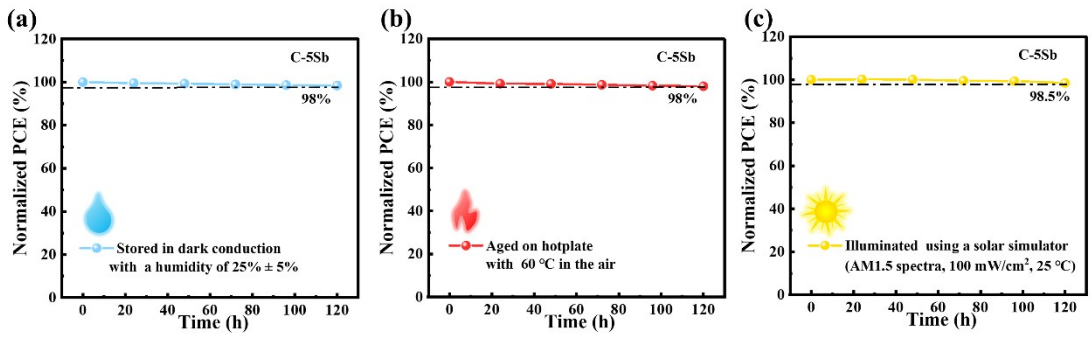

Fig. S11 (a) Moisture stability, (b) Heat stability and (c) Light stability of cell C-5Sb.

Table S5. The summary of typical solution-processed CIGSe solar cells prepared by different doping methods.

Absorber	Doping method	*V*oc (V)	*J*sc (mA/cm^2)	FF (%)	Eg (eV)	PCE (%)	Thickness (μm)	PCE/μm (%)	Ref.
CIGSSe	Na doping	0.6	26.8	63.6	1.18	10.3	2	5.15	S8
CIGSSe	Na and K Codoping	0.62	30.8	62.6	/	12.0	1.3	9.23	S9
CIGSSe	K doping	0.62	33.1	73.5	1.16	15	1.3	11.53	S10
CIGSSe	K doping	0.66	33.61	72.65	1.24	16.02	1.24	12.91	S11
CIGSSe	K doping	0.643	37.75	73.06	1.14	17.74	2	8.87	S12
CIGSSe	Ag doping	0.63	34.44	72.9	1.19	15.82	1.2	13.18	S13
CIGSSe	**Sb doping**	**0.638**	**35.5**	**72.08**	**1.18**	**16.33**	**1.2**	**13.6**	**This work**

References

[S1] Metzger W K, Repins I L, Romero M, et al. Recombination kinetics and stability in polycrystalline Cu(In, Ga)Se_2 solar cells. Thin Solid Films, 2009, 517(7): 2360-2364.

[S2] Kim S T, Larina L, Yun J H, et al. Surface passivation and point defect control in Cu(In,Ga)Se $_2$ films with a Na_2S post deposition treatment for higher than 19% CIGS cell performance. Sustainable energy & fuels, 2019, 3(3): 709-716.

[S3] Li J, Zhang Y, Zhao W, et al. A temporary barrier effect of the alloy layer during selenization: tailoring the thickness of $MoSe_2$ for efficient $Cu_2ZnSnSe_4$ solar cells. Advanced Energy Materials, 2015, 5(9): 1402178.

[S4] Li J, Deng B, Zhu H, et al. Rear interface modification for efficient Cu(In,Ga)Se_2 solar cells processed with metallic precursors and low-cost Se vapor. Solar Energy Materials and Solar Cells, 2018, 186: 243-253.

[S5] Hegedus S S, Shafarman W N. Thin-film solar cells: device measurements and analysis. Progress in Photovoltaics: Research and Applications, 2004, 12(2-3): 155-176.

[S6]Gao Z R, Xiong Y C, Wang J W, et al. Efficiency improvement for post-sulfurized CIGS solar cells enabled by in situ Na doping. Journal of Energy Chemistry, 2025, 101: 324-332.

[S7] Xu X, Li L, Yang M, et al. Localized state effect and exciton dynamics for monolayer WS_2. Optics Express, 2021, 29(4): 5856-5866.

[S8] Uličná S, Welch L M, Abbas A, et al. Sodium doping of solution-processed amine-thiol based CIGS solar cells by thermal evaporation of NaCl. Progress in Photovoltaics: Research and Applications, 2021, 29(5): 546-557.

[S9] Alruqobah E H and Agrawal R. Potassium Treatments for Solution-Processed Cu(In, Ga)(S,Se)$_2$ Solar Cells. ACS Applied Energy Materials, 2020, 3(5):4821-4830.

[S10] Kim J H, Kim M K, Gadisa A, et al. Morphological–Electrical Property Relation in Cu(In, Ga)(S,Se)$_2$ Solar Cells: Significance of Crystal Grain Growth and Band Grading by Potassium Treatment. Small, 2020,16(48), 2003865.

[S11] Zhao Y H, Gao Q Q, Yuan S J, et al. Defects passivation and crystal growth promotion by solution-processed K doping strategy toward 16.02% efficiency Cu(In,Ga)(S,Se)$_2$ solar cells. Chemical engineering journal, 2022,436,135008.

[S12] Mina M S, Kim S, Enkhbat T, et al. High Efficiency Aqueous Solution Sprayed CIGSSe Solar Cells: Effects of Zr4+-Alloyed In_2S_3 Buffer and K-Alloyed CIGSSe Absorber. Advanced Functional Materials, 2022,32(46),2206561.

[S13] Zhao Y, Yuan S, Kou D, et al. High efficiency CIGS solar cells by bulk defect passivation through Ag substituting strategy. ACS applied materials & interfaces, 2020, 12(11), 12717-12726.